Biophysical Chemistry 185 (2014) 70–78

Contents lists available at ScienceDirect

Biophysical Chemistry

journal homepage: http://www.elsevier.com/locate/biophyschem

Comparative structural and conformational studies on H43R and W32F mutants of copper–zinc superoxide dismutase by molecular dynamics simulation

Gurusamy Muneeswaran [a], Subramanian Kartheeswaran [b], Kaliappan Muthukumar [c], Christopher D. Dharmaraj [b], Chandran Karunakaran [a,*]

[a] Biomedical Research Laboratory, Department of Chemistry, VHNSN College (Autonomous), Virudhunagar, 626001 Tamilnadu, India
[b] Biomedical Research Laboratory, Department of Computer Science, VHNSN College (Autonomous), Virudhunagar, 626001 Tamilnadu, India
[c] Institute for Theoretical Physics, Goethe University, Frankfurt Am Main, Germany

HIGHLIGHTS

- H43R exhibits greater mobility at Zn-binding and electrostatic loops.
- Dimer interface interaction in H43R is weakened compared to that of WT and W32F.
- Distances between the highly conserved amino acids increase for H43R.
- The decreased activity should be attributed to the opening of active channel in H43R.

GRAPHICAL ABSTRACT

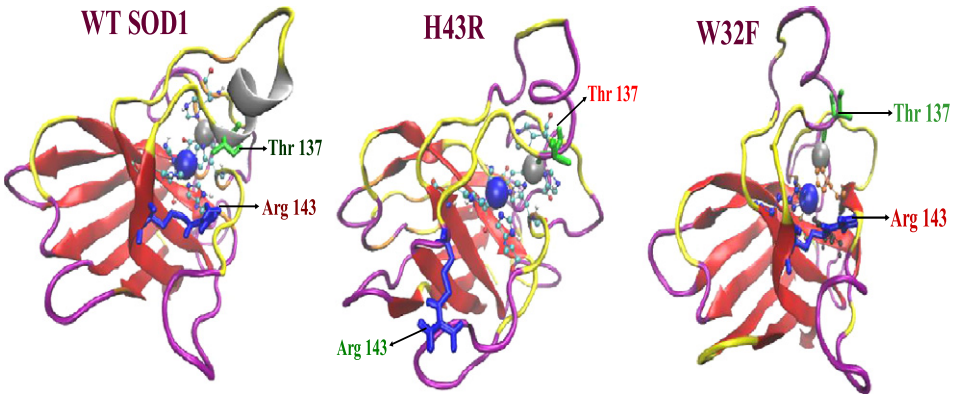

ARTICLE INFO

Article history:
Received 18 September 2013
Received in revised form 30 November 2013
Accepted 30 November 2013
Available online 11 December 2013

Keywords:
SOD1
fALS
W32F
H43R
Molecular dynamics
GROMACS

ABSTRACT

Recently, mutations in copper–zinc superoxide dismutase (SOD1) have been linked to familial amyotrophic lateral sclerosis (fALS), a progressive neurodegenerative disease involving motor neuron loss, paralysis and death. It is mainly due to protein misfolding and aggregation resulting from the enhanced peroxidase activity of SOD1 mutants. In this study, we have carried out a 20 ns molecular dynamics simulation for wild type (WT), H43R and W32F mutated SOD1's dimer and compared their structure and conformational properties by extracting several quantitative properties from the trajectory to understand the pathology of fALS disease. Our results show considerable differences in H43R compared to WT and W32F mutated SOD1, such as increasing distances between the critical residues results in open conformation at the active site, strong fluctuations in the important loops (Zinc and electrostatic loops) and weakening of important hydrogen bonds especially between N (His 43/Arg 43) and carbonyl oxygen (His 120) in agreement with the experimental report. The calculated buried surface area of dimer interface for WT, H43R and W32F are 682, 726 and 657 $Å^2$ respectively, representing the loss of dimerization in H43R. Essential dynamics reveal that overall motions of WT and W32F are mainly involved in three to four eigenvectors, but in H43R the overall motions are mainly in the first eigenvector. These data thus provide a unifying description for the structural destabilization, enhanced peroxidase activity, loss of dismutation activity and increase in aggregation propensity in the pathology of fALS diseases.

* Corresponding author at: Biomedical Research Laboratory, Department of Chemistry, VHNSN College (Autonomous), Virudhunagar, 626001 Tamilnadu, India. Tel.: +91 04562 280154; fax: +91 04562 281338.
E-mail address: ckaru2000@gmail.com (C. Karunakaran).

0301-4622/$ – see front matter © 2013 Elsevier B.V. All rights reserved.
http://dx.doi.org/10.1016/j.bpc.2013.11.010

1. Introduction

Copper–zinc superoxide dismutase (SOD1) is a metalloenzyme, abundantly found in the intracellular cytoplasmic space of aerobic organisms and is responsible for defending cells from oxidative damage [1]. SOD1 is a functional homodimer, (molecular weight of ca. 32 kDa) with each monomer containing one Cu(II) and Zn(II) ions that are bridged by an anionic histidinato ligand. The Cu(II) ion in SOD1 is further coordinated to three other histidine residues in a distorted square pyramidal geometry, while Zn(II) is bound to two histidine and an aspartate residue in a distorted tetrahedral geometry [2]. Each monomer of SOD1 forms an eight-stranded antiparallel β-barrel. The β-barrel of SOD1 is protected against self-aggregation by having each end of the dimer covered by well ordered electrostatic and zinc binding loops [3]. Further, these two extended loop regions form a wall for the channel formed between the surfaces of enzyme to the active site [4].

SOD1 catalyzes the disproportionation of superoxide anions into molecular oxygen and hydrogen peroxide and the widely accepted catalytic mechanism [5] involves the two following steps,

$$SOD\text{-}Cu^{2+} + O_2^{\cdot -} \text{---------} > SOD\text{-}Cu^{+} + O_2 \quad (1)$$

$$SOD\text{-}Cu^{+} + O_2^{\cdot -} + 2H^{+} \text{--------} > SOD\text{-}Cu^{2+} + H_2O_2. \quad (2)$$

Early biochemical studies, measuring the SOD1 activity in amyotrophic lateral sclerosis (ALS) patients, suggested that the reduction or the loss of enzyme activity and an increase in the peroxidase activity can be suppressed through post-translational modifications (such as the attainment of copper and zinc ions, formation of disulphide bond and dimerization) that help in the regaining of enzymatically active quaternary structure [6,7]. Mutations affecting the post-translational modifications in human SOD1 were identified as an important cause for approximately 20% of fALS [3,8–10]. The fALS-associated mutants do not essentially reduce the activity of SOD1, but gain some new activities such as peroxidase/thiol oxidase activity that might also lead to protein misfolding followed by its aggregation [11–14].

More recently, pulsed EPR and NMR spectroscopic studies were used to establish the oxidation of His 43 residue during peroxidase activity of SOD1 resulting in the loss of enzyme activity [15]. It has been found that the fALS sites are associated not only with the active site His residues, but also with the integrity of the β-barrel fold, the dimer interface, and other structural features [6]. In addition to the metal-bound His residues in the active site, His 43 is only the residue located in the vicinity of the active site, (ca. 11 Å away from the Cu (II) site) [15] positioned at an opening of the β-barrel and stabilizes the ends of the compact structure of β-barrel through its hydrophobic packing interactions with the nearby residues [16,17]. His 43 also assists with the exact orientation of the Arg 143 side chain with respect to the Cu active site by forming a hydrogen bond bridge [16,17]. Therefore, His 43 to Arg mutation in human SOD1 (H43R), enhances the disruption of the Thr39-His43-His120 hydrogen bond bridge that indeed alters the position and orientation of Arg 143 residue, resulting in a reduced stability of SOD1 protein structure leading to protein aggregation [6]. Further, H43R mutation has been identified in patients of fALS [9,10,16].

Similarly, Trp 32 is located on the surface of human SOD1 and the oxidation of Trp 32 occurs in vivo as a natural modification to SOD1 leading to peroxide-induced aggregation [18]. The enhanced peroxidase activity of human SOD1, resulting in the formation of a tryptophanyl radical by the reaction with carbonate anion radical ($CO_3^{\bullet -}$), has been found to cause protein aggregation [13,14]. Further, mutating Trp 32 with Phe (W32F) slows down the rate of oxidative modification [13,14,18] that has been found to decrease the cytotoxicity in motor neuronal cell culture model and the rate of aggregation of SOD1[14].

Information about the dynamical properties of these mutants of SOD1 is crucial in understanding their role in protein activities/aggregation on a molecular level. Since, crystal structures of SOD1 mutants give only the static behavior, molecular dynamics (MD) simulations were used as an alternative tool for probing the structural as well as conformational changes due to mutations [3]. MD simulations reveal atomic-level insights which remain inaccessible by present high resolution experimental methods, and that are expected to shed light on the unresolved issues connecting the protein's dynamics and structure to its biological activities [19]. Studies describing the structure and dynamics of WT and selectively mutated SOD1's are available [3,20–26]. More recently, Schmidlin et al. [27] performed MD simulations on A4V mutated SOD1 and demonstrated the structural changes to monomeric SOD1 but have not focused on describing the dynamical behavior of these two mutations (H43R and W32F) and their relation to protein aggregation and its stability. Indeed, this is essential in understanding the pathology of fALS diseases and therefore by using classical molecular dynamics, we address here the dynamical properties of these mutated systems and explain several properties and their relation to the protein activities/aggregation on a molecular level.

2. Computational methods

The starting co-ordinates of the WT SOD1 dimer (pdb entry 1spd) at 2.4 Å resolution were obtained from the protein data bank [28]. We have constructed H43R and W32F mutants using the interactive computer graphics package Swiss pdb viewer v 3.6 [29] by substituting His 43 residue with Arg and Trp 32 residue with Phe in the WT crystal structure. Molecular dynamics (MD) simulations were carried out using the GROMACS 4.5.3 [30] package using GROMOS96 [31] 43a1 force field for all residues and metal ions. The protonation state was treated with the help of optimal H-bonding conformation. The standard GROMOS96 charges were used for all the atoms except for the residues of the active site, for which the partial atomic charges calculated from ab initio methods reported in Ref. [32] were employed. Each structure was fully solvated with SPC cubic water in a box with side's 6.939 nm × 4.719 nm × 4.190 nm with box angles 90° for each side. The whole dimeric enzyme of WT, H43R and W32F mutated SOD1's was embedded in 22639, 22642 and 22647 water molecules respectively.

The steepest descent algorithm was used for energy minimization and the maximum step size for energy minimization considered was 0.01 nm. The tolerance used in this simulation was 6000 kJ/mol/nm. The WT protein and W32F mutant both have a net charge of −5 e, while the H43R mutant has a net charge of −4 e. Precise simulation of protein dynamics needs the inclusion in the model of, at least, a neutralizing counter ion's atmosphere, therefore in this work, five and four Na^+ ions were added by replacing solvent molecules with the highest electrostatic potential for WT, W32F and H43R mutants respectively, thus the investigated proteins have a net charge of zero. Initially, position-restrained MD was carried out for 200 ps which restrains the position of atoms in the protein and allows the distribution of solvent in the system. The LINCS algorithm was used to constrain all bonds [33] and SETTLE algorithm [34] for solvent distribution.

In our simulations, the temperature was maintained at 300 K by weak coupling to an external temperature bath and the simulation is continued for 20 ns (including the equilibration steps) for each WT, H43R and W32F mutated SOD1's. A time step of 2 fs was used and the data were collected every 500 fs. A twin range cut-off was used for the calculation of the non-bonded interactions. The short range cut-off radius was set to 0.9 nm and the long range cut-off radius was set to 1.4 nm for both columbic and Lennard–Jones interactions. The electrostatic interaction was handled by the particle-mesh Ewald (PME) method [35]. The distances measured at the active site metals after 20 ns of MD simulations are shown in Supplemental Table S1. It reveals that the geometry of the active site is maintained, and shows that the set of parameters employed for the metal ions and their ligands are reliable for studying the dynamical behavior of this molecule.

The essential dynamics (ED) is obtained by diagonalizing the covariance matrix, which is built from the atomic fluctuations in a MD trajectory where overall translational and rotational motions have been removed, [31,36–38]

$$C_{ij} = \left(\frac{X_i - X_{i,0}}{X_j - X_{j,0}}\right) \quad (3)$$

where **X** are the x, y and z coordinates of the atoms fluctuating around their average positions ($\mathbf{X}_0$) and <…> denotes an average over time. To construct the protein covariance matrices, we have used Cα atoms trajectory, as it has been shown that the Cα atoms contain the necessary information to reasonably describe large concerted motion of the proteins [26]. Upon diagonalization of the covariance matrix, a set of eigenvalues and eigenvectors is obtained. The eigenvectors of the covariance matrix correspond to directions in a 3N-dimensional space (where N is the number of Cα atoms), and motions along a single eigenvector correspond to concerted fluctuations of atoms. Our system contained 306 Cα atoms, having 918 position coordinates for each case. The eigenvalues of the covariance matrix represent the total mean square fluctuation of the system along the corresponding eigenvectors. If the eigenvectors are ordered according to their decreasing eigenvalues, the first one describes the largest scale correlated motions, whereas the last one will correspond to small-amplitude vibrations [39].

3. Results and discussion

Over 130 mutations to SOD1 have been identified in fALS patients, and the clusters of fALS related point mutations are found around the β-barrel opening [9,10], at the dimer interface regions and other structural features [6,40]. His 43 is positioned just behind the active site and mutating His 43 to Arg resulting in reduced stability of SOD1 leading to protein aggregation [6,40]. Trp 32 is far away from the active site and represents one of the normally occurring oxidative modifications that promotes aggregation and toxicity of proteins [18]. However, the rates of oxidation-induced aggregation of WT SOD1 were decreased by replacing Trp 32 with Phe [14,15,18]. In order to examine the structural stability and dynamical changes in the structure of WT, H43R and W32F mutated SOD1's dimer, we report here several geometrical and conformational properties obtained from the MD trajectories. The calculated structural features exhibit good correspondence with the X-ray measurements and are listed in Table 1.

3.1. Root mean square deviation (RMSD)

The RMSD of the backbone and the Cα atoms of the investigated proteins are extracted from the simulated trajectory, which are then compared to understand the relative stability. The plot, describing the RMSD of the investigated proteins backbone over the course of simulation time is shown in Fig. 1. RMSD values of the backbone atoms with respect to the initial structure indicates that within 5 ns a stable behavior is reached, showing that the WT protein is equilibrated. The equilibration time for W32F mutant is 2 ns and 7 ns for H43R. The average RMSD of backbone and Cα atoms of WT are 0.2787 nm and 0.2828 nm, while for H43R and W32F mutated SOD1, the values are 0.2606 nm and 0.2657 nm & 0.2371 nm and 0.2430 nm respectively. In H43R mutated SOD1, both the backbone and the Cα RMSD (data not shown) exhibit significantly less flexibility up to 6.5 ns compared to WT, but after which a considerable change in RMSD, (from 0.20 nm to 0.30 nm) was observed that has been found to remain constant in the rest of simulation window. This sudden increase in backbone and Cα RMSD's is due to the disruption of major loops, β-barrel and dimer interface, indicating a structural instability. However, in W32F mutated SOD1 the backbone and Cα RMSD's decrease considerably when compared to WT and thus the stability is increased.

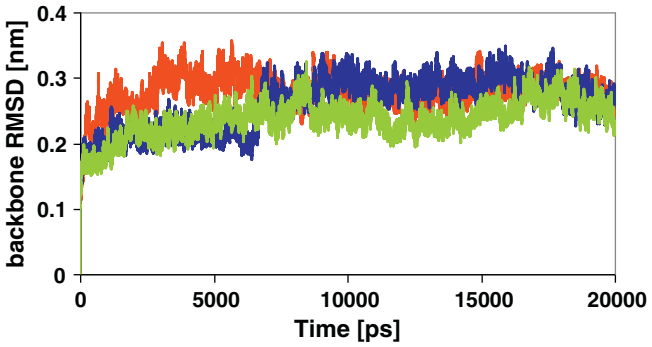

Fig. 1. Evolution of structural properties over time backbone RMSD: Red—WT, Blue—H43R and Green—W32F SOD1's.

3.2. Radius of gyration (Rg)

The Rg is defined as the mass-weighted root mean square distance of a collection of atoms from their common center of mass and this analysis gives insight into overall globularity of the protein. The average values of radius of gyration Rg (Cα) for WT, H43R and W32F mutated SOD1 are 1.91, 1.93 and 1.92 nm respectively. The value (average Rg (Cα)) computed for WT SOD1 is in good agreement with the already reported value of 1.89 nm [35]. Furthermore, the average values of Rg (protein) for WT, H43R and W32F mutated SOD1 are 1.94, 1.96 and 1.95 nm respectively. These values indicate that both WT and the mutated SOD1 have similar globularity.

3.3. Root mean square fluctuations (RMSF)

The differences in the mobility of residues can be understood from the values of RMSF (Chain A & B) relative to the average structure and are shown in Fig. 2 (a) and (b). The RMSF differences show that the dynamics of the core were different for WT, H43R and W32F mutated SOD1's. The RMSF analysis of critical residues for WT and both the mutated SOD1 indicate that the two subunits Chain A and Chain B exhibit dissimilar dynamical behaviors and their active site residues exhibit distinct fluctuations. This asymmetric behavior of the individual subunit has been well documented for WT SOD1 dimer [7].

In H43R mutated SOD1, we find in Chain B that there are two loop regions comprising residues 48–85 (Zinc loop/loop IV) and 121–143 (Electrostatic loop/loop VII) show larger fluctuations for the entire simulation window, indicating a strong deformation or disorder in these loops. Since, loop IV in SOD1 is located close to the interface between two monomers, the observed fluctuations might also have a crucial impact in maintaining the dimer structure of SOD1 [7]. This supports the larger deviation of RMSD values (protein's backbone and Cα) for H43R mutation compared to WT and W32F mutated SOD1.

Table 1
Geometrical properties of SOD1 compared with the X-ray structure.

Geometrical properties	MD average	X-ray structure
Accessible surface of protein (WT)	14198 Å^2	14251 Å^2
Accessible surface area of protein (H43R)	13971 Å^2	13959 Å^2
Dimer interface (WT)	682 Å^2	~640 Å^2[a]
Radius of gyration (WT Cα-atoms)	1.91 nm	1.96 nm[b]
Surface area of residue-43 (H43R)	256 to 291 Å^2	271 to 293 Å^2[c]
Solvent accessibility of Leu38	2164 to 2286 Å^2	Increases[c]
Solvent accessibility of Thr39	1222 to 1231 Å^2	Increases[c]
Solvent accessibility of Glu40	532 to 536 Å^2	Increases[c]

[a] P.A. Doucette et al., J. Biol. Chem, 279 (2004), 54558–54566.
[b] G. Chillemi et al., Biophys. J, 73 (1997), 1007–1018.
[c] M. DiDonato et al., J. Mol. Biol, 332 (2003), 601–615.

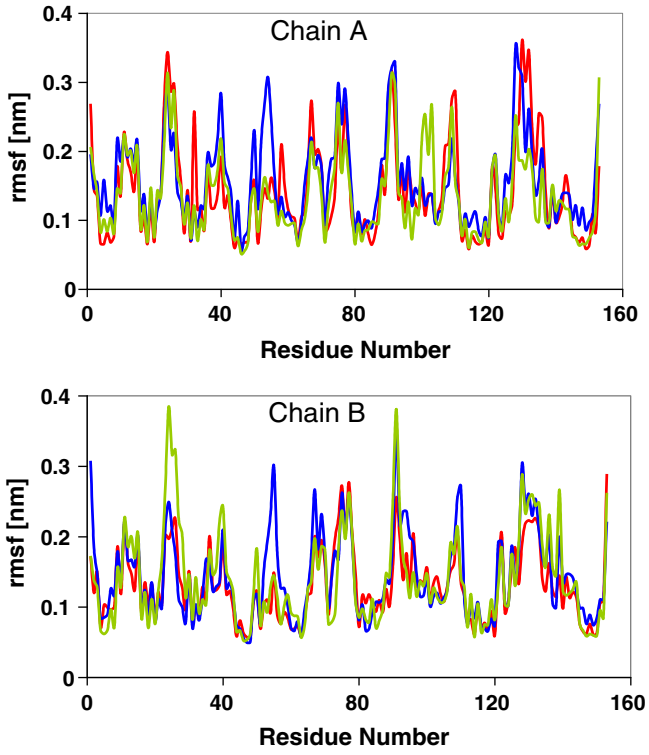

Fig. 2. RMSF of backbone atoms as a function of amino acids: Red—WT, Blue—H43R and Green—W32F SOD1's.

Furthermore, it has been reported that loop VII produces an optimal electrostatic field for the uptake of superoxide anion radical [7] and the deformation occurring as a result of this mutation disrupts the orientation of metal-ligands for the dismutation reaction that consequently reduces its catalytic activity. In W32F mutated SOD1, the loop containing residues 48–85 (Zinc loop/loop IV) and 121–143 (Electrostatic loop/loop VII) exhibit similar fluctuations as WT, explaining minor differences in the catalytic activity of these two proteins.

3.4. Solvent accessible surface area (SASA)

The average SASA values for WT (−5 e), H43R (−4 e) and W32F (−5 e) mutated SOD1's are 14,198, 13,971 and 14,131 Å^2 respectively. The average SASA value calculated from this simulation is in good agreement with the reported experimental value of 14120 Å^2 [6]. Comparison of calculated values indicates that the residues in H43R mutated SOD1 are effectively packed compared to WT and W32F SOD1.

The buried solvent-accessible surface area of residue His 43/Arg43 in H43R mutated SOD1 increases from 256 Å^2 to 291 Å^2. Further, we have also calculated the SASA for Leu 38 and its nearby residues (Thr 39 and Glu 40) because these are considered to play an important role in stabilizing the β-barrel [16]. Moreover, the side chain of Leu 38 is in van der Waals contact with His 43, whose amide chain is linked to catalytically important Arg 143 by forming a hydrogen bond bridge [16]. The total solvent accessibilities of Leu 38, Thr 39 and Glu 40 for WT are 2164 Å^2, 1222 Å^2 and 532 Å^2 while for H43R mutated SOD1they are 2286 Å^2, 1231 Å^2 and 536 Å^2 respectively. This increase in the solvent accessibility of Leu 38 and its nearby residues relative to WT might alter the positions and orientations of Leu 38 and Arg 143 side chains, leading to a distortion of the structural stability and also reduce the catalytic activity (see Fig. S1in the supplemental material). Further, this could be a general feature of fALS mutants, since similar packing imperfections were already identified in the fALS SOD1 mutant A4V, which affect the dimer interface and other β-barrel end [6,41]. In W32F mutant, we find no evidence of substantial change in SASA values of individual residues compared to WT, signifying that the dimer interface and β-barrel end are preserved in a similar way to WT SOD1.

3.5. Solvent accessible surface in the dimer interface

Dimerization of the individual monomer subunits increases the stability of SOD1 [42] and therefore mutations that perturb the interaction between these monomers and a perturbation at the dimer interface decrease the overall stability of the protein. The dimer interface is formed by reciprocal contacts between the C-terminal β-strand and residues from the disulphide loop from each monomer [43]. Our MD results of buried SASA in the dimer interface for WT (−5 e), H43R (−4 e) and W32F (−5 e) mutants are 682 Å^2, 726 Å^2 and 657 Å^2 respectively. The increase in the value for H43R mutated SOD1, indicates that the reciprocal contacts between the C-terminal β-strand and residues from the disulphide loop are relatively weakened compared to WT and W32F SOD1. We have also analyzed the average structures of chain B for WT, H43R and W32F mutated SOD1 in our simulations and present in Fig. 3. Comparison of these structures indicates clearly that the β-barrel of H43R mutated SOD1 undergoes the largest structural fluctuations indicating that this part of the protein undergoes severe deformations. It has been shown by electron and atomic force microscopic techniques that the loss of dimerization and partial loss of the β-barrel

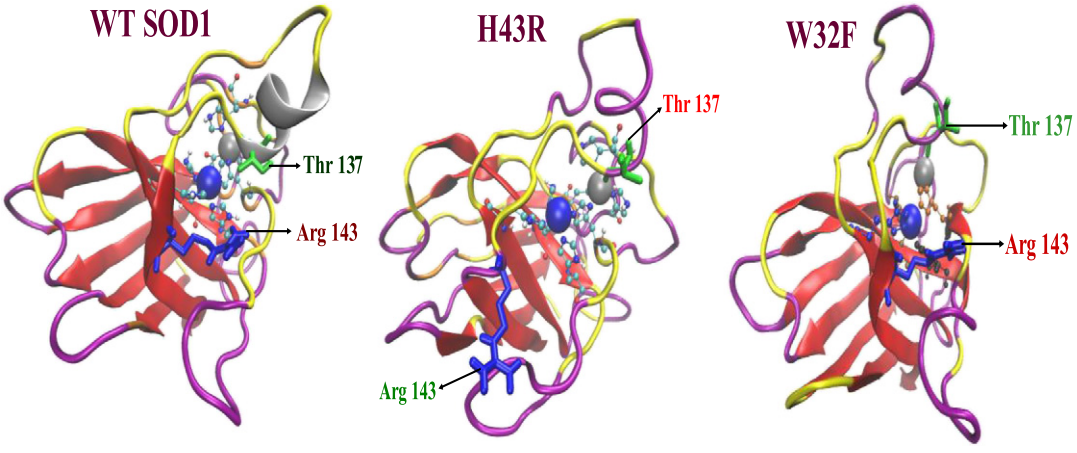

Fig. 3. The changes in the overall structures of SOD1 and mutants after 20 ns MD simulations, the β-sheets are colored as red.

result in fibril aggregation [44]. In the case of W32F mutated SOD1, the reciprocal contacts are strengthened compared to WT, representing that the dimer interface and β-barrel are maintained in W32F mutated SOD1, in agreement with experimental observations [15,23].

3.6. Secondary structure analysis

The secondary structure of proteins is the local polypeptide backbone structure, which is typically expressed by the Ramachandran plot [45]. The Ramachandran plots for WT, H43R and W32F mutated SOD1 are shown in Fig. 4. The most allowed conformational regions of Ramachandran space are colored blue, and partially allowed conformational regions are colored green. In SOD1, the disulphide loop (Cys 57 and Cys 146) can influence the conformation of the enzymatically important residue, Arg 143, through a hydrogen bonding network. Portions of this loop contribute to the dimer interface, leading to the possibility that the disulphide loop influences the protein dimerization and thereby the SOD1 secondary structure [6]. Fig. 4 very clearly reveals that in WT and W32F mutated SOD1, the catalytically important Arg 143 residue is within the most allowed regions while, in H43R mutated SOD1, Arg 143 residue has moved to partially allowed region. Furthermore, one of the disulphide loop residue Cys 57 is found within the partially allowed regions for both the WT and W32F mutated SOD1, but in H43R mutated SOD1, Cys 57 has moved to the disallowed region illustrating a strong perturbation in the structure that might be one of the cause of destabilization. Also we find that Cys 146 is placed in most allowed regions for WT and W32F mutated SOD1, and it has moved to the less favorable region in H43R mutated SOD1. Further we have also calculated phi and psi values of Cys 146, Cys 57 and Arg 143 for WT, H43R and W32F mutated SOD1's from secondary structure analysis and are shown in Supplemental Table 2. These results possibly illustrate that the secondary structure of H43R mutated SOD1exhibited more structural changes that might enhance the aggregation property of the proteins, compared to WT and W32F mutated SOD1.

3.7. H-bonding network

A complex network of hydrogen bonding determines the orientation of the metal ligands and active site channel configuration, which is essential in maintaining a high catalytic efficiency of SOD1 [44]. Experimentally M. DiDonato et al. [6] reported that, in the WT crystal structure, the His 43 side chain forms a series of hydrogen bond between the main chain carbonyl oxygen atoms of Thr 39, His 120 and Glu 121, and is found lying near to Leu 38. The Arg 43 side-chain keeps up the His 43 hydrogen bonds with the carbonyl oxygen atoms of Thr 39 and Glu 121. However, the Arg 43 mutation results in the loss of a hydrogen bond that existed between His 43 N and the carbonyl oxygen of His 120. The distances between the N (His 43/Arg 43) and the carbonyl oxygen of His 120 for WT, H43R and W32F mutants are 0.4999 nm, 0.6536 nm and 0.4905 nm respectively. These results are presented in Table 2, obviously indicating the loss of hydrogen bond between Arg 43 N and the carbonyl oxygen of His 120 in agreement with the experimental work done by M. Di Donato et al. This loss of one main-chain to side-chain hydrogen bond in H43R mutant might destabilize the structure by disrupting the orientations of the metal ligands, Leu 38 and Arg 143 in conjunction with a loss of catalytic activity and in agreement with the SASA analysis. This observation strongly suggests that His 43 is an important part of the highly efficient catalytic machinery of SOD1. But in W32F mutated SOD1, the hydrogen bond between His 43 N and the carbonyl oxygen of His 120 is preserved, signifying the increase of its catalytic activity.

In WT SOD1 dimer, the monomers forming the dimeric molecule are linked by hydrogen bonds formed between i) subunit A Gly51N–subunit B Ile151O and ii) subunit A Gly114O–subunit B Ile151N [4]. Analysis of distance variations in these hydrogen bonds observed in our MD simulations are shown in Table 2, which indicates that the

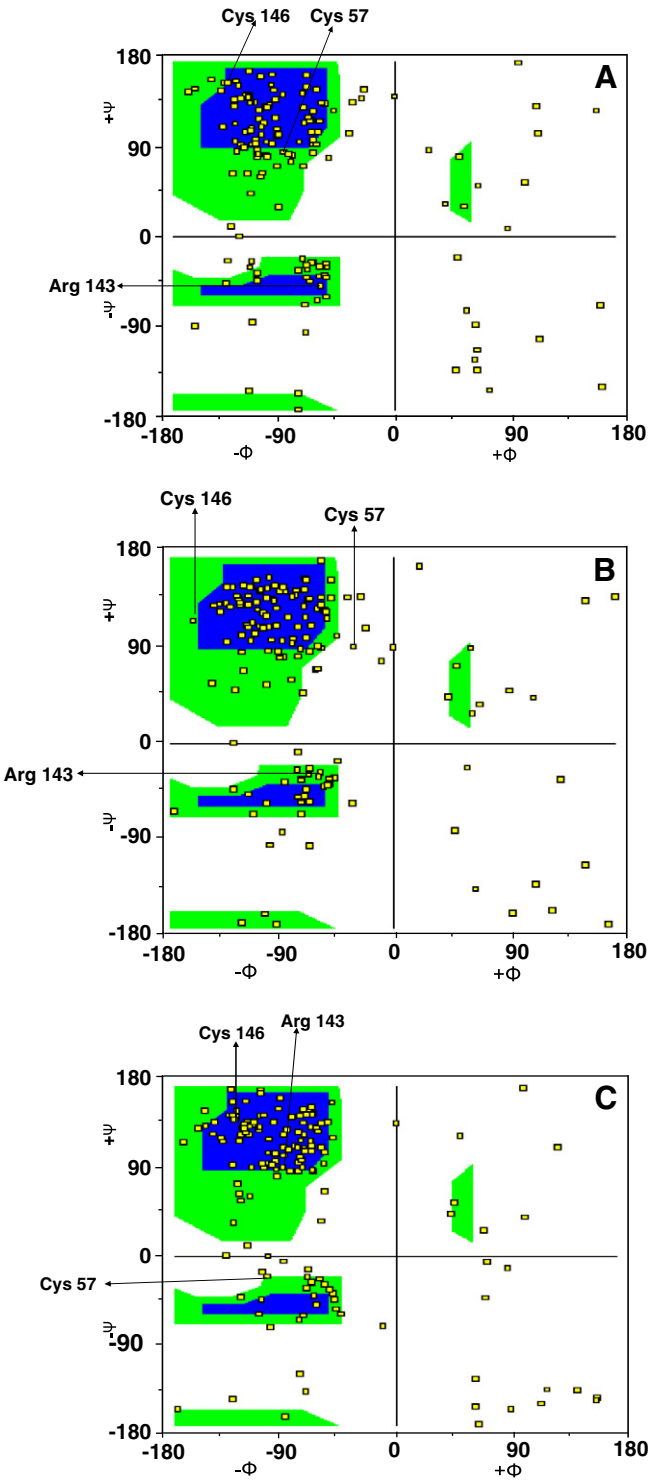

Fig. 4. Ramachandran plots of the backbone torsion angles for WT and mutated SOD1's.

Table 2
Hydrogen bonding distance variation analysis.

Atoms	WT (nm)	H43R mutant (nm)	W32F mutant (nm)
O His 120–N His 43/Arg 43	0.4999	0.6536	0.4905
O Thr 39–N His 43/Arg 43	0.4345	0.4324	0.4361
O Glu 121–N His 43/Arg 43	0.3389	0.3468	0.3248
AGly51N-Bile151O	0.2803	0.2844	0.2607
AGly114O-Bile151N	0.3055	0.3097	0.2841

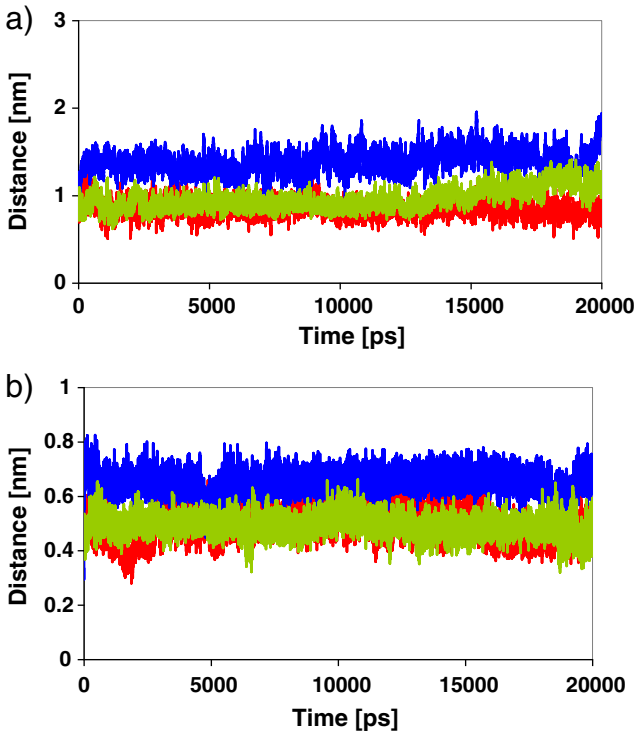

Fig. 5. Distances between a) Cζ Arg 143 and Cβ Thr 137, b) O His 120 and ND1 His 43/Arg43: Red—WT, Blue—H43R, Green—W32F.

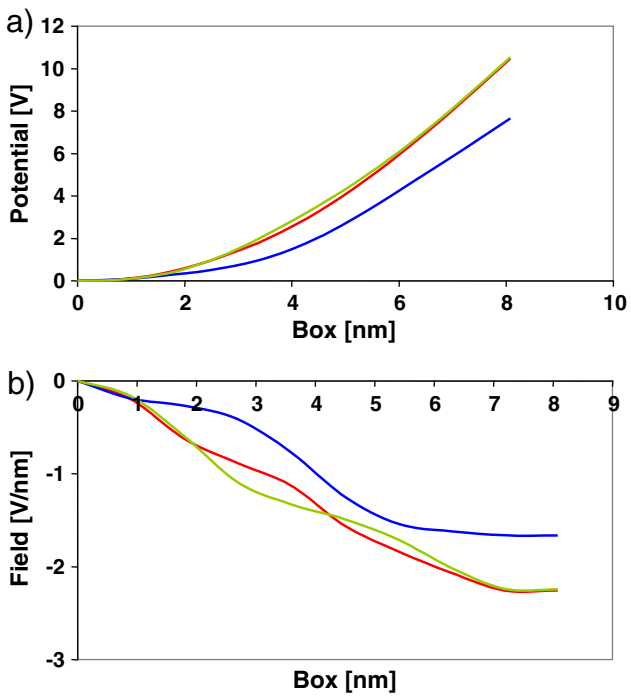

Fig. 6. Plot of (a) Electrostatic Potential and (b) Electric Field as a function of across the box dimensions: Red—WT, Blue—H43R, Green—W32F.

distances of selected hydrogen bonds are increased in H43R, mutated SOD1 than WT. This reveals that the dimeric interface in the H43R mutated SOD1 is considerably weakened, supporting a structural destabilization. In the case of W32F mutated SOD1 the distances of hydrogen bonds are decreased more than WT SOD1 indicating a strengthening of dimeric interface and thus increased structural stability. These observations are consistent with our conclusions from SASA analysis.

3.8. Distance variation analysis between the critical residues

In addition to its unique bimetallic active site structure, SOD1 has exceptionally high catalytic efficiency [17] in converting superoxide anions into molecular oxygen and hydrogen peroxide. The catalytic efficiency is attributed to the positive and negative charged residues on the protein surface and in the active site channel, which steers the superoxide anion radical towards the active site. This is maintained by the correct alignment of critical residues [17]. The distance between the Cζ Arg 143 and Cβ Thr 137, the two strictly conserved amino acid residues, determines the narrowest section of the active site channel [21] and so, we have measured the distances between critical residues (Cζ Arg 143 — Cβ Thr 137, and O His 120 and ND1 His 43) in WT and mutated SOD1 and the results are shown in Fig. 5 (a) and (b). The results illustrate that upon mutation, the two groups move apart from the channel which is enhanced in H43R mutated SOD1 compared to W32F mutated SOD1 in both chains A and B.

The key point should be that the Cζ Arg 143 and Cβ Thr 137 and O His 120 and ND1 His 43 distances change significantly in H43R but the fluctuations remain uniform throughout the entire simulation. This could disturb the narrowest section of the active site channel and produce less attraction for the incoming superoxide anion radical, thus the enzymatic activity is reduced in H43R mutated SOD1 which might result in an enhanced peroxidase activity compared to WT and W32F mutated SOD1. Further, we have also listed the distance variation between the critical residues in the active site environment for chain-A and chain-B in Table 3 which also suggest that the dynamic behaviors of the two monomers are instantaneously asymmetrical and in agreement with reported experimental work [2]. The asymmetrical behavior is more pronounced for H43R mutated SOD1.

Table 3
Distance variation of critical and conserved residues for Chain A (values for Chain B are given in parentheses).

Distance between the residues	WT (nm)	H43R mutant (nm)	W32F mutant (nm)
Cζ Arg143	0.8915 (0.8488)	1.0195 (1.3871)	0.9082 (0.9650)
Cζ Arg143	1.0060 (0.9173)	0.7909 (1.0368)	0.7607 (0.7338)
$N\eta_1$ Arg143	1.0112 (0.9315)	0.8271 (1.0750)	0.8264 (0.7886)
$N\eta_2$ Arg143	1.0958 (0.9947)	0.8606 (1.1026)	0.8080 (0.7836)
Nζ Lys136	1.1622 (1.3729)	1.6067 (1.5746)	1.6260 (1.6358)
Nζ Lys136-OE1 Glu132	1.0415 (0.5792)	0.5806 (0.5507)	0.5752 (0.6047)
O1 Thr137	0.7763 (0.7763)	0.8648 (0.8675)	0.8810 (0.9194)
OD1 Asp124	0.3097 (0.3239)	0.3185 (0.2942)	0.3176 (0.3314)
OD2 Asp124	0.3808 (0.4438)	0.4842 (0.3673)	0.4975 (0.4205)

3.9. Electrostatic potential and electric field calculations

The electrostatic interactions play an important role in the SOD1 catalytic function. At long range, it steers the incoming superoxide anion radical to the active site, and at short range, it furnishes the specific local interactions for catalysis. The superoxide is electrostatically attracted by the Arg 143 residue to the copper atom [5]. For these reasons, we have calculated the electrostatic potentials across the box for

Table 4
Electrostatic potential calculations.

	WT (V)	H43R (V)	W32F (V)
Dimeric protein	3.72	2.59	3.81
Active site	−2.30	−3.04	−2.63
Copper atom	−0.7784	−1.0374	−0.8680
Arg143 residue	−1.5153	−1.7992	−1.3807

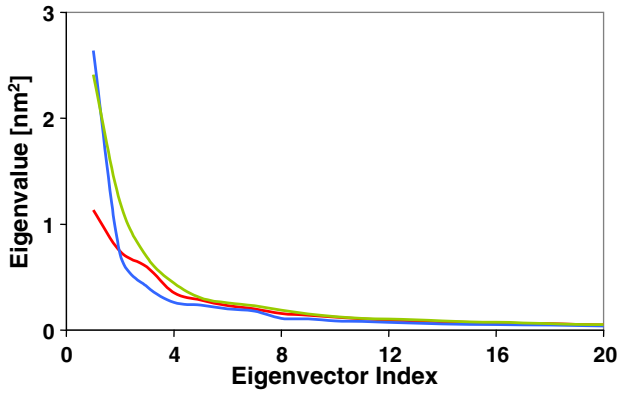

Fig. 7. Plot of eigenvalues corresponding to eigenvector index for the first twenty modes of motion; Red—WT, Blue—H43R and Green—W32F SOD1's.

WT, H43R and W32F mutated SOD1's. Plots of electrostatic potential and electric field as a function of across the box dimensions are shown in Fig. 6 (a) and (b). The average electrostatic potentials for the whole dimeric protein (WT and mutants), active site, copper atom and catalytically important Arg 143 residue are reported in Table 4. The average electrostatic potentials of whole dimeric WT (−5 e), H43R (−4 e) and W32F (−5 e) mutated SOD1's are 3.72 V, 2.59 V and 3.81 V respectively. These values indicate that WT and W32F SOD1's show almost a similar behavior, while H43R mutated SOD1 reveals a significant different behavior compared to WT SOD1. To understand this effect, we have also calculated the electrostatic potential for the active site of these proteins which are found to be −2.30 V, −3.04 V and −2.63 V for WT, H43R and W32F mutated SOD1 respectively. The less positive electrostatic potential of whole dimer and more negative value of active site for H43R mutation indicate a lesser reduced affinity for the incoming superoxide anion towards the active site supporting a loss or reduction of catalytic activities of the protein. The analysis electric field across the box also reveals that the WT and W32F mutated SOD1's show similar behavior, but H43R mutated SOD1 exhibits a significantly different behavior compared to WT. These results might also be relevant in explaining the dismutation reaction and fibrous aggregation of WT and both the mutated enzymes.

3.10. Essential dynamics analysis

Essential dynamics (ED) is a method that utilizes principal component analysis (PCA) on the actual coordinates of the system and thus gives the essential motion of the protein in phase space [31]. The structural fluctuations corresponding to each eigenvector are generated by a different combination of the motions involving subdomains including the major loops and β-barrel [26]. After the removal of rotational motions, a covariance matrix was constructed for WT, H43R and W32F mutated SOD1 and the eigenvalues using Eq. (1). The eigenvalues are plotted in Fig. 7 against the corresponding eigenvector index for the first twenty modes of motion at different trajectory lengths. Fig. 7 shows that the first eigenvector in WT is 1.334 nm^2, while for H43R and W32F mutated SOD1 they are 2.6396 nm^2 and 2.4129 nm^2 respectively indicating that for the first eigenvector, the mutated enzymes undergo larger motion compared to WT. For the successive eigenvectors up to fifth, H43R mutated SOD1 undergo less motion than WT, while the W32F mutated SOD1 experience enhanced motion compared to WT. However, in the remaining fifteen eigenvectors we find a similar behavior for these three proteins suggesting that the motions occur mainly along very few directions in the essential subspace, but with different amplitude for concerted motions for these three proteins.

This analysis shed further insight about the nature of the motions represented by eigenvectors in H43R mutated SOD1. The major

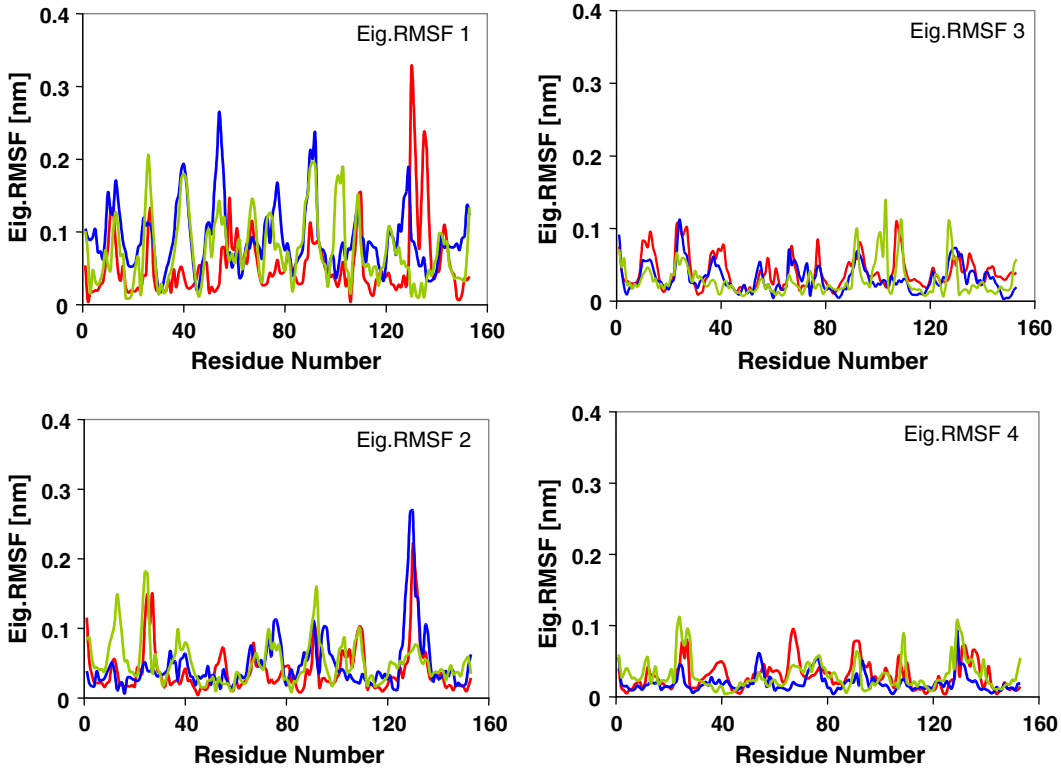

Fig. 8. RMSF per atom of eigenvectors as a function of Cα atoms; Red—WT, Blue—H43R and Green—W32F SOD1's.

collective modes of fluctuations involving the loops and β-barrel are mainly occurred in the first eigenvector for H43R mutated SOD1. These results are significant in understanding the behavior of H43R mutated SOD1. However in the case of WT and W32F mutated SOD1, the major protein motion occurred not only in the first eigenvector but also included a few more eigenvectors.

Eigen RMSF per atom of eigenvectors as a function of Cα atoms is shown in Fig. 8 indicating the Cα displacements along the four main eigenvectors. The essential motions identified are different for WT and the mutated proteins. Fig. 8 clearly indicates that in H43R mutated SOD1, there are two loop regions viz., 48–85 (Zinc loop/loop IV) and 121–143 (Electrostatic loop/loop VII). They explore a wide conformational space since their motions have large amplitude along all the first four most important directions of the essential space. In WT and W32F mutants, the residues 48–85 (Zinc loop/loop IV) and residues 121–143 (Electrostatic loop/loop VII) undergo lesser movements. These results reveal that the concerted motions of these two loops decreased considerably in WT and W32F mutant and these structural fluctuations are related to the results developed from other analyses of the present MD simulations.

4. Conclusions

The dynamics of H43R and W32F mutated SOD1 have been investigated to analyze their properties quantitatively, to understand the changes in structural and conformational features that can be used to explain the role of these mutants in fALS pathology. Upon H43R mutation in SOD1, several features viz., large fluctuations in the electrostatic and Zn-binding loops followed by rapid loss of β-sheet conformations, the increase in distance between highly conserved amino acid residues especially at the narrow active site, the increase in SASA at the dimer interface, and the loss of important hydrogen bonds, result in considerable changes in the structure, conformation and functions of the mutated protein. Essential dynamic analysis reveals that the overall motions are mainly due to the first eigenvector for H43R and three to four eigenvectors for WT and W32F mutated SOD1. These results clearly account for the observed loss in the dismutation activity and enhanced peroxidase activity. Further, this study explains the dissociation of dimer especially in H43R and thus provides insight into the mechanism of mutation–protein aggregation relationship in fALS pathology.

Acknowledgments

This work was supported by the UGC, New Delhi, India (F.No. 39-690/2010 (SR)) and the Managing Board of Virudhunagar Senthikumara Nadar College (Autonomous), Virudhunagar, Tamilnadu, India.

Appendix A. Supplementary data

Supplementary data to this article can be found online at http://dx.doi.org/10.1016/j.bpc.2013.11.010.

References

[1] I. Fridovich, Superoxide dismutase, Annu. Rev. Biochem. 44 (1975) 147–159, http://dx.doi.org/10.1146/annurev.bi.44.070175.001051.
[2] M.A. Hough, S.S. Hasnain, Crystallographic structures of bovine copper–zinc superoxide dismutase reveal asymmetry in two subunits: functionally important three and five coordinate copper sites captured in the same Crystal, J. Mol. Biol. 287 (1999) 579–592, http://dx.doi.org/10.1006/jmbi.1999.2610.
[3] R.W. Strange, C.W. Yong, W. Smith, S.S. Hasnain, Molecular dynamics using atomic-resolution structure reveal structural fluctuations that may lead to polymerization of human Cu–Zn superoxide dismutase, Proc. Natl. Acad. Sci. U. S. A. 104 (2007) 10040–10044, http://dx.doi.org/10.1073/pnas.0703857104.
[4] M.A. Hough, J.G. Grossmann, S.V. Antonyuk, R.W. Strange, P.A. Doucette, J.A. Rodriguez, L.S. Whitson, P.J. Hart, L.J. Hayward, J.S. Valentine, S.S. Hasnani, Dimer destabilization in superoxide dismutase may result in disease-causing properties: structures of motor neuron disease mutants, Proc. Natl. Acad. Sci. U. S. A. 101 (2004) 5976–5981, http://dx.doi.org/10.1073/pnas.0305143101.
[5] M.D. Alessandro, M. Aschi, M. Paci, A.D. Nola, A. Amadei, Theoretical modeling of enzyme reaction chemistry: the electron transfer of the reduction mechanism in CuZn superoxide dismutase, J. Phys. Chem. A 108 (2004) 16255–16260, http://dx.doi.org/10.1021/jp0487861.
[6] A.M. DiDonato, L. Craig, M.E. Huff, M.M. Thayer, R.M.F. Cardoso, C.J. Kassmann, T.P. Lo, C.K. Bruns, E.T. Powers, J.W. Kelly, E.D. Getzoff, J.A. Tainer, ALS mutants of human superoxide dismutase form fibrous aggregates via framework destabilization, J. Mol. Biol. 332 (2003) 601–615, http://dx.doi.org/10.1016/S0022-2836(03)00889-1.
[7] F. Arnesano, L. Banci, I. Bertini, M. Martinelli, Y. Furukawa, T.V. O'Halloran, The unusually stable quaternary structure of human Cu, Zn-superoxide dismutase 1 is controlled by both metal occupancy and disulfide status, J. Biol. Chem. 279 (2004) 47998–48003, http://dx.doi.org/10.1074/jbc.M406021200.
[8] E.L. Shipp, F. Cantini, I. Bertini, J.S. Valentine, L. Banci, Dynamic properties of the G93A mutant of copper–zinc superoxide dismutase as detected by NMR spectroscopy: implications for pathology of familial amyotrophic lateral sclerosis, Biochemistry 42 (2003) 1890–1899, http://dx.doi.org/10.1021/bi026704y.
[9] D.R. Rosen, T. Siddique, D. Patterson, D.A. Figlewicz, P. Sapp, A. Hentati, D. Donaldson, J. Goto, J. O'Regan, H.X. Deng, Z. Rahmani, A. Krizus, D. McKenna-Yasek, A. Cayabyab, S.M. Gatson, R. Berger, R.E. Tanzi, J.J. Halperin, B. Herzfeldt, R. Van der Bergh, W.Y. Hung, T. Bird, G. Deng, D.W. Mulder, C. Smyth, N.G. Laing, E. Soriano, M.A. Pericak-Vance, J. Haines, G.A. Rouleau, J.S. Gusella, H.R. Horvitz, R.H. Brown Jr., Mutations in Cu/Zn superoxide dismutase gene are associated with familial amyotrophic lateral sclerosis, Nature 362 (1993) 59–62, http://dx.doi.org/10.1038/362059a0.
[10] M.E. Cudkowicz, D. McKenna-Yasek, P.E. Sapp, W. Chin, B. Geller, D.L. Hayden, D.A. Schoenfeld, B.A. Hosler, H.R. Horvitz, R.H. Brown, Epidemiology of mutations in superoxide dismutase in amyotrophic lateral sclerosis, Ann. Neurol. 41 (1997) 210–221.
[11] C. Karunakaran, H. Zhang, J. Joseph, W.E. Antholine, B. Kalyanaraman, Thiol oxidase activity of copper, zinc superoxide dismutase stimulates bicarbonate dependent peroxidase activity *via* formation of a carbonate radical, Chem. Res. Toxicol. 18 (2005) 494–500, http://dx.doi.org/10.1021/tx049747j.
[12] J.P. Julien, Amyotrophic lateral sclerosis: unfolding the toxicity of the misfolded, Cell 104 (2001) 581–591.
[13] C. Karunakaran, H. Zhang, J.P. Crow, W.E. Antholine, B. Kalyanaraman, Direct probing of copper active site and free radical formed during bicarbonate-dependent peroxidase activity of bovine and human SOD1, J. Biol. Chem. 279 (2004) 32534–32540, http://dx.doi.org/10.1074/jbc.M314272200.
[14] H. Zhang, C. Anderkopoulos, J. Joseph, C. Karunakaran, H. Karoui, J.P. Crow, B. Kalyanaraman, Bicarbonate-dependent peroxidase activity of human Cu, Zn-superoxide dismutase induces covalent aggregation of protein, J. Biol. Chem. 278 (2003) 24078–24089, http://dx.doi.org/10.1074/jbc.M314272200.
[15] C. Karunakaran, J. McCracken, F.C. Peterson, W.E. Antholine, B.F. Volkman, B. Kalyanaraman, Oxidation of histidine residues in SOD1 by bicarbonate-stimulated peroxidase and thiol oxidase activities: pulse EPR and NMR studies, Biochemistry 49 (2010) 10616–10622, http://dx.doi.org/10.1021/bi1010305.
[16] H.X. Deng, J.A. Tainer, H. Mitsumoto, A. Ohnishi, X. He, W.Y. Hung, Y. Zhao, T. Juneja, A. Hentati, T. Siddique, Two novel SOD1 mutations in patients with familial amyotrophic lateral sclerosis, Hum. Mol. Genet. 4 (1995) 1113–1116, http://dx.doi.org/10.1093/hmg/4.6.1113.
[17] L. Banci, I. Bertini, F. Cramaro, R. Del Conte, M.S. Viezzoli, The solution structure of reduced dimeric copper zinc superoxide dismutase, the structural effects of dimerization, European, J. Biochem. 269 (2002) 1905–1915, http://dx.doi.org/10.1046/j.1432-1033.2002.02840.x.
[18] D.M. Taylor, B.F. Gibbs, E. Kabashi, S. Minotti, H.D. Durham, J.N. Agar, Tryptophan 32 potentiates aggregation and cytotoxicity of a SOD1 mutant associated with familial amyotrophic lateral sclerosis, J. Biol. Chem. 282 (2007) 16329–16335, http://dx.doi.org/10.1074/jbc.M610119200.
[19] J.D. Perlmutter, A.R. Braun, J.N. Sachs, Curvature dynamics of α-Synuclein familial Parkinson disease mutants molecular simulations of the micelle-and bilayer-bound forms, J. Biol. Chem. 284 (2009) 7177–7189, http://dx.doi.org/10.1074/jbc.M808895200.
[20] R.J.F. Branco, P.A. Fernandes, M.J. Ramos, Molecular dynamics simulations of the enzyme Cu, Zn superoxide dismutase, J. Phys. Chem. B 110 (2006) 16754–16762, http://dx.doi.org/10.1021/jp056855l.
[21] L. Banci, P. Carloni, G.L. Penna, P.L. Orioli, Molecular dynamics studies on superoxide dismutase and its mutants: the structural and functional role of Arg 143, J. Am. Chem. Soc. 114 (1992) 6994–7001, http://dx.doi.org/10.1021/ja00044a007.
[22] M. Falconi, M.E. Stroppolo, P. Cioni, G. Starmbini, A. Sergi, M. Ferrario, A. Desideri, Dynamics-function correlation in Cu, Zn superoxide dismutase: a spectroscopic and molecular dynamics simulation study, Biophys. J. 80 (2001) 2556–2567, http://dx.doi.org/10.1016/S0006-3495(01)76227-3.
[23] S.D. Khare, N.V. Dokholyan, Common dynamical signatures of familial amyotrophic lateral sclerosis-associated structurally diverse Cu, Zn superoxide dismutase mutants, Proc. Natl. Acad. Sci. U. S. A. 103 (2006) 3147–3152, http://dx.doi.org/10.1073/pnas.0511266103.
[24] A. Amadei, M.D. Alessandro, M. Paci, A.D. Nola, A. Aschi, On the effect of point mutation on the reactivity of CuZn Superoxide dismutase: a theoretical study, J. Phys. Chem. B 110 (2006) 7538–7544, http://dx.doi.org/10.1021/jp057095h.
[25] F. Ding, N.V. Dokholyan, Dynamical role of metal ions and the disulfide bond in SOD1 folding and aggregation, Proc. Natl. Acad. Sci. U. S. A. 105 (2008) 19696–19701, http://dx.doi.org/10.1073/pnas.0803266105.

[26] G. Chillemi, M. Falconi, A. Amadei, G. Zimatore, A. Desideri, A.D. Nola, The essential dynamics of Cu, Zn superoxide dismutase: suggestion of intersubunit communication, Biophys. J. 73 (1997) 1007–1018, http://dx.doi.org/10.1016/S0006-3495(97)78134-7.
[27] T. Schmidlin, B.K. Kennedy, V. Daggett, Structural changes to monomeric CuZn superoxide dismutase caused by the familial amyotrophic lateral sclerosis-associated mutation A4V, Biophys. J. 97 (2009) 1709–1718, http://dx.doi.org/10.1016/j.bpj.2009.06.043.
[28] H.X. Deng, A. Hentati, J.A. Tainer, Z. Iqbal, A. Cayabyab, W.Y. Hung, et al., Amyotrophic lateral sclerosis and structural defects in Cu, Zn superoxide dismutase, Science 261 (1993) 1047–1051, http://dx.doi.org/10.1126/science.8351519.
[29] N. Guex, A. Diemand, T. Schwede, M.C. Peitsch, Swiss-Pdb Viewer, V 3.62000.
[30] D. van der Spoel, E. Lindahl, B. Hess, G. Groenhof, A.E. Mark, H.J. Berendsen, GROMACS: fast, flexible, and free, J. Comput. Chem. 26 (2005) 1701–1718.
[31] W.F. van Gunsteren, S.R. Billeter, A.A. Eising, P.H. Hunenberger, P. Kruger, A.E. Mark, W.R.P. Scott, I.G. Tironi, Biomolecular Simulation: The Gromos 96 Manual and User Guide, Hochschulverlag AG an der Zurich, Zurich, Switzerland, 1996.
[32] J. Shen, C.F. Wong, S. Subramaniam, T.A. Albright, J.A. McCammon, Partial electrostatic charges for the active center of Cu, Zn superoxide dismutase, J. Comput. Chem. 11 (1990) 346–350, http://dx.doi.org/10.1002/jcc.540110309.
[33] B. Hess, H. Bekker, H.J.C. Berendsen, J.G.E.M. Fraaije, Lincs: a linear constraint solver for molecular simulations, J. Comput. Chem. 18 (1997) 1463–1472, http://dx.doi.org/10.1002/(SICI)1096-987X(199709)18:12<1463::AID-JCC4>3.0.CO;2-H.
[34] S. Miyamoto, P.A. Kollman, SETTLE: an analytical version of the SHAKE and RATTLE algorithms for rigid water molecules, J. Comput. Chem. 13 (1992) 952–962, http://dx.doi.org/10.1002/jcc.540130805.
[35] U. Essmann, L. Perera, M.L. Berkowitz, T. Darden, H. Lee, L.G. Pederson, A smooth particle meshes Ewald potential, J. Chem. Phys. 103 (1995) 8577–8592, http://dx.doi.org/10.1063/1.470117.
[36] H.J.C. Berendsen, D. van der Spoel, R. van Drunen, GROMACS: a message-passing parallel molecular dynamics implementation, Comput. Phys. Commun. 91 (1995) 45–56, http://dx.doi.org/10.1016/0010-4655(95)00042-E.
[37] E. Lindahl, B. Hess, D. van der Spoel, GROMACS 3.0 a package for molecular simulation and trajectory analysis, J. Mol. Model. 7 (2001) 306–317, http://dx.doi.org/10.1007/s008940100045.
[38] D. van der Spoel, E. Lindahl, B. Hess, A.R. Van Buuren, E. Apol, P.J. Meulenhoff, D.P. Tieleman, A.L.T.M. Sijbers, A.K. Feenstra, R. Van Druunen, H.J.C. Berendsen, Groningnen Machine for Molecular Simulations BIOSON Research Institute, Groningnen, the Netherlands, 2004.
[39] A. Amadei, A.B. Linssen, H.J.C. Berendsen, Essential dynamics of proteins, Proteins 17 (1993) 412–425, http://dx.doi.org/10.1002/prot.340170408.
[40] A. Toyama, Y. Takahashi, H. Takeuchi, Catalytic and structural role of a metal-free histidine residue in bovine Cu–Zn superoxide dismutase, Biochemistry 43 (2004) 4670–4679, http://dx.doi.org/10.1021/bi049767k.
[41] G.S.A. Wright, S.V. Antonyuk, N.M. Kershaw, R.W. Strange, S.S. Hasnain, Ligand binding and aggregation of pathogenic SOD1, Nat. Commun. 4 (2013) 1758, http://dx.doi.org/10.1038/ncomms2750.
[42] P.A. Doucette, L.J. Whitson, X. Cao, V. Schiri, B. Demeler, J.S. Valentine, J.C. Hansen, P.J. Hart, Dissociation of human copper–zinc superoxide dismutase dimers using chaotrope and reductant, J. Biol. Chem. 279 (2004) 54558–54566, http://dx.doi.org/10.1074/jbc.M409744200.
[43] E.A. Proctor, F. Deng, N.V. Dokholyan, Structural and thermodynamic effects of post-translational modifications in mutant and wild type Cu, Zn superoxide dismutase, J. Mol. Biol. 408 (2011) 555–567, http://dx.doi.org/10.1016/j.jmb.2011.03.004.
[44] J.J.P. Perry, D.S. Shin, E.D. Getzoff, J.A. Tainer, The structural biochemistry of the superoxide dismutases, Biochim. Biophys. Acta 1804 (2010) 245–262, http://dx.doi.org/10.1016/j.bbapap.2009.11.004.
[45] G.N. Ramachandran, V. Sasiskharan, Conformation of polypeptides and proteins, Adv. Protein Chem. 23 (1968) 283–437.